Supporting Information

Selective Heterogeneous Transfer Hydrogenation from Tertiary Amines to Alkynes

Gabriel J. Roeder,[a,‡] H. Ray Kelly,[b,‡] Guoju Yang,[a] Thomas J. Bauer,[a] Gary L. Haller,[a,c]
Victor S. Batista[b] and Eszter Baráth[a,*]

[a]Technische Universität München, Department of Chemistry and Catalysis Research Center, Lichtenbergstraβe 4, Garching, D-85748, Germany
[b]Yale University, Department of Chemistry, 225 Prospect Street, P.O. Box 208107, New Haven CT 06520, USA
[c]Yale University, Department of Chemical and Environmental Engineering, 9 Hillhouse Ave., P.O. Box 208286, New Haven, CT 06520, USA

[‡]These authors contributed equally.
*E-mail: eszter.barath@tum.de

CONTENT

Experimental procedures, materials

Chemicals The following chemicals were used as received, without any additional purification or further treatment: anhydrous *p*-xylene (Sigma-Aldrich ≥ 99.0%), CH_2Cl_2 (Sigma-Aldrich ≥ 99.8%), mesitylene (Sigma-Aldrich 99.0%), 5-decyne (Sigma-Aldrich 98.0%), *cis*-5-decene (TCI Chemicals > 95%), *trans*-5-decene (Sigma-Aldrich 99.0%), decane (Sigma-Aldrich ≥ 99.0%), diphenylacetylene (Sigma-Aldrich 98.0%), *trans*-stilbene (Sigma-Aldrich 96.0%), *cis*-stilbene (Sigma-Aldrich 96.0%), 1,2-diphenylethane (Sigma-Aldrich 96.0%), 1-phenyl-1-propyne (Sigma-Aldrich 99.0%), *trans*-1-phenyl-1-propene (Sigma-Aldrich 99.0%), cis/*trans*-1-phenyl-1-propene (TCI Chemicals > 95%), propylbenzene (Sigma-Aldrich 98.0%), 1-phenyl-1-hexyne (Sigma-Aldrich 99.0%), 1-phenylhexane (Sigma-Aldrich 97.0%), cyclohexylacetlyene (Sigma-Aldrich 98.0%), vinylcyclohexane (Sigma-Aldrich 97.0%), 4-ethynylanisole (Sigma-Aldrich 97.0%), 4-vinylanisole (Sigma-Aldrich 97.0%), 2-ethynylanisole (Sigma-Aldrich 97.0%), 2-vinylanisole (Sigma-Aldrich 98.0%), *N,N*-diisopropylethylamine (Sigma-Aldrich ≥ 98.0%), 1-ethylpyrrolidine (Sigma-Aldrich 97.0%), 1,10-phenanthroline (Sigma-Aldrich ≥ 99.0%), nitrogen (Westfalen > 99.999%), hydrogen (Westfalen > 99.999%) and argon (Westfalen > 99.996%). The catalysts Pd/C (10 wt%) (Sigma-Aldrich CAS/205699), Pt/C (10 wt%) (Sigma-Aldrich CAS/205958) were activated prior to their use.[1]

Catalyst activation The commercial catalysts (Pd/C, Pt/C) were activated before usage.[1] The reduction was performed in flowing H_2 at 120°C for 1 h, then the temperature was increased to 400°C with a heating rate of 1 °C min^{-1} and held for 3 hours (flow rate of H_2: 100 mL min^{-1}), the samples were then flushed with N_2 for 1 h before collection. Afterwards, the catalysts were immediately transferred into the glovebox with a very brief exposure to air.

Catalytic reactions The catalytic reactions were carried out in a Schlenk-tube under inert conditions.[1] All the reagent materials, the catalyst Pd/C (10 wt%): 106.42 mg (1 mmol Pd/C (0.1 mmol Pd)) or Pt/C (10 wt%): 195.08 mg (1 mmol Pt/C (0.1 mmol Pt)), *p*-xylene (1.5 mL), the corresponding amount of amines (4.4 mmol), the substrate (1.0 mmol; 5-decyne (**1**); 1-phenyl-1-propyne (**2**); 1-phenyl-1-hexyne (**3**); diphenylacetylene (**4**); hexylacetylene (**5**); 4-ethynylanisole (**6**); 2-ethynylanisole (**7**)) were added to the Schlenk-tube in a glove box. The reaction mixture was kept under inert conditions and heated to the corresponding temperature (reaction temperature/140°C; temperatures for kinetic measurements: 90°C, 110°C, 140°C). After the required reaction time, the reaction mixture was cooled to room temperature (reaction time 14h; different time regimes for kinetic measurements). Sequentially, the catalyst was filtered out and an aliquot of the reaction mixture (50 µL) was taken and diluted with *p*-xylene (1 mL), mesitylene (10 µL) was added to the mixture as internal standard (IS) (for isomer identification analysis of substrate **1** depending from the analysis method, mesitylene or butylcyclohexane was used as internal standard). The samples were analysed by GC-MS (*Agilent 7890B* gas chromatograph with *Agilent 5977A* mass spectrometer). The carbon balance of transfer hydrogenation for all the substrates was better than 98%.

GC-MS The filtered and prepared liquid samples were analysed *via* an *Agilent 7890B* gas chromatograph equipped with a flame ionization detector (FID) and an *Agilent 5977A* mass spectrometer. Mesitylene was used as the internal standard. The liquid sample (1 µL) was injected into a HP-5 MS column (30 m × 0.32 mm × 0.25 µm) at an inlet temperature of 250°C. The column temperature was initially held at 50°C for substrates **1**, **2**, **5** and at 80°C for substrates **3**, **4**, **6**, **7** for the duration of 1 min. The temperature was then increased to 80°C for **1**, **2** (65°C for **5**) at a rate of 4°C min^{-1} or to 200°C for **3**, **4**, **6**, **7** at a rate of 10°C min^{-1} and held at that temperature for 2 min. Afterwards, the temperature was slowly increased to 85°C for **1**, **2** (75°C for **5**) at a rate of 0.5°C min^{-1} or to 210°C for **3**, **4**, **6**, **7** at a rate of 1°C min^{-1}. After holding the temperature for another two minutes the temperature was increased to a final 150°C for **1**, **2** at a rate of 5°C min^{-1} (for **5** at a rate of 10°C min^{-1}) or to 250°C (**3**, **4**, **6**, **7**) at a rate of 10°C min^{-1}. The column flow was maintained constant at 1.3 mL min^{-1} for the measurement. The FID was operated at 280°C (for **5-7** 300°C). Identification of the components was performed by using the retention times of commercially available pure substances. Quantification of reactants was analysed *via* the FID-signal. *Cis/trans* isomer identification of substrate **3** was cross-checked with previously published data.[2]

For the product distribution analysis of substrate **1**, the following procedure was used: column/ *VF200ms* (30 m × 0.25 mm × 0.25 µm). The FID was operated at 270°C. Carrier gas/ N_2, 0.61 mL min^{-1}; injection: 1 µl at 270°C, split 30:1, butylcyclohexane (10 µL) as internal standard. Temperature program: starting

temperature was 60°C which was held for 1 min, at a rate of 5°C min^{-1} the temperature was increased to 100°C, at a rate of 20°C min^{-1} the temperature increased further to 250°C and was held for 3 min.

Atomic Absorption Spectroscopy (AAS) Elemental analysis of the samples were performed by atomic absorption spectroscopy on a *ICE 3500 AAS (Thermo Fisher Scientific)* equipped with a GF 95 graphite furnace to determine the Pd, Pt, content of the catalysts. The samples were dissolved in a solution of perchloric acid (72%) and nitro-hydrochloric acid at its boiling point before the measurement.

Transmission electron microscopy (TEM) TEM measurements were performed on a *JEOL JEM-2011* equipment at 120 kV. The average particle size and its standard deviation was calculated based on the Pd and Pt particle size distribution of 300 metal particles measured in at least five different particle domains of the catalyst.

XRD X-Ray powder diffraction patterns were recorded with a *PANalytical Empyrean System* (Cu Kα, Kα1 = 0.154059 nm, Kα2 = 0.154442 nm) operated at 45 kV/40 mA, in the 2θ range of 10–90° with a step size of 0.013130° and a scan speed of 0.061071° s^{-1}. (Standards used for data analysis: (Pd) JCPDS card no. 46-1043; (Pt) JCPDS card no. 04-0802.)

Particle size distribution and XRD pattern of Pd/C and Pt/C

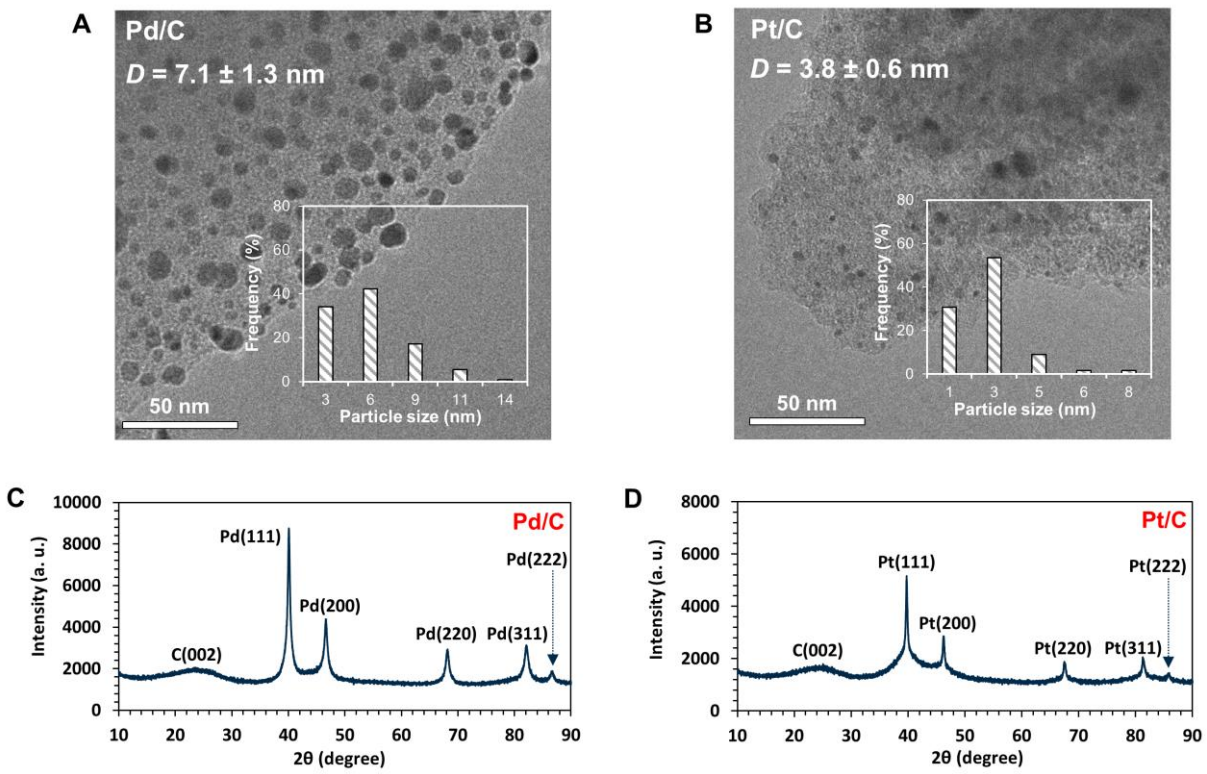

Figure S1. Particle size distribution of Pd/C (**A**) and Pt/C (**B**) *via* TEM analysis, XRD pattern of Pd/C (**C**) and Pt/C (**D**).

For the particle size distribution each metal was estimated based on at least 300 metal particles from five different particle domains of each catalyst. The average particle size is 7.1 ± 1.3 nm and 3.8 ± 0.6 nm for Pd/C and Pt/C, respectively.

BET surface analysis Specific surface area of the support was determined from nitrogen adsorption-desorption isotherms recorded on an automated *PMI Sorptomatic 1990* instrument at liquid nitrogen temperature (77 K). The samples were outgassed in vacuum (p = 1×10^{-3} mbar) for 2 h at 475 K prior to adsorption. The specific surface areas were calculated by applying the *B.E.T. theory*, the *t-plot method* was used to determine the micropore volumes and mesopore surface areas, while mesopore volumes was determined using the *B.J.H. theory*.

H_2 Chemisorption The active carbon supported metal (Pd, Pt) was pre-treated at 573 K under 0.1 MPa H_2 for 1 h, followed by evacuation in vacuum for 1 h. After the temperature was cooled to 298 K, the H_2 chemisorption and physisorption were subsequently determined in a pressure of H_2 from 5 to 350 Torr. Then, the physisorbed H_2 was removed by outgassing the sample at 298 K for 1 h. The concentration of chemisorbed hydrogen on the metal was obtained by extrapolating the isotherm to zero Torr of H_2 pressure. The metal (Pd, Pt) dispersion and TOF were deduced by assuming an average H/metal ratio of 1.

Mode of calculations

Conversion = (mole of converted reactant / mole of the starting reactant) (× 100 (%)). **Yield** = the ratio of the amount of reaction product and the amount of a starting material (× 100 (%)). **Selectivity** = the ratio of the amount of reaction product and the amount of a converted feedstock material (× 100 (%)). **The initial reaction rate** was deduced from the slope of the linear fit to the conversion versus reaction time plot in the linear region at low conversions (< 25%). **TOF** = mole of converted reactant / (mole of accessible metal sites × reaction time) (mol $mol_{(surf.\ metal)}^{-1}$ s^{-1} which is shortened as s^{-1}). Accessible metal sites (mol $g_{(cat)}^{-1}$) were calculated by the normalization of the catalyst amount to metal dispersion and metal loading. **The carbon balance** = (mole of carbon in the product / mole of carbon of starting reactant) (× 100 (%)).

Representative GC spectra

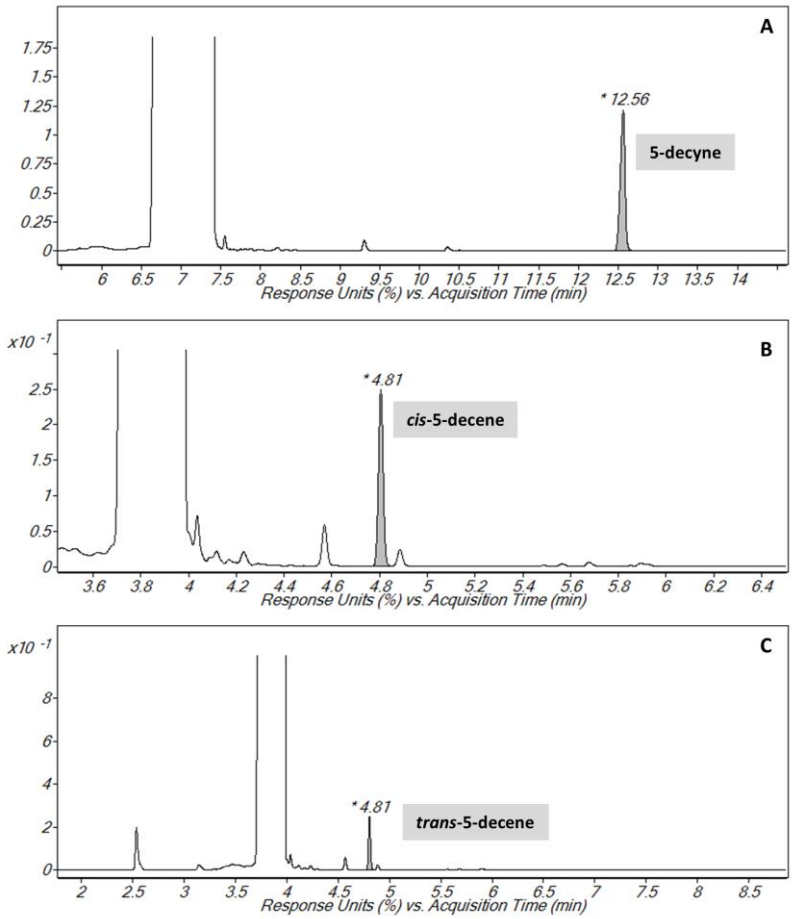

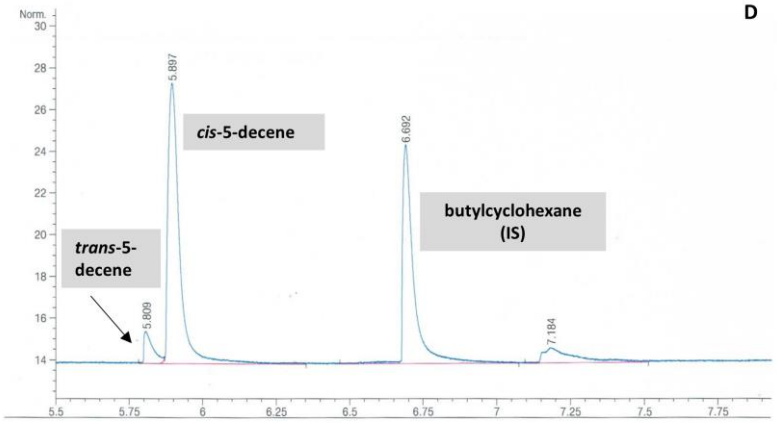
D
Norm.
5.897
6.692
5.809
7.184
cis-5-decene
butylcyclohexane (IS)
trans-5-decene

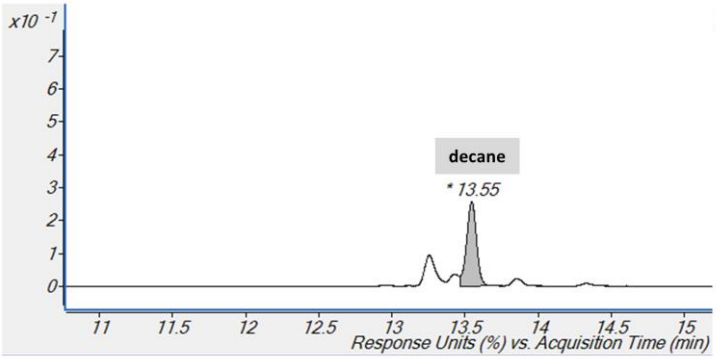
E
x10 -1
decane
* 13.55
Response Units (%) vs. Acquisition Time (min)

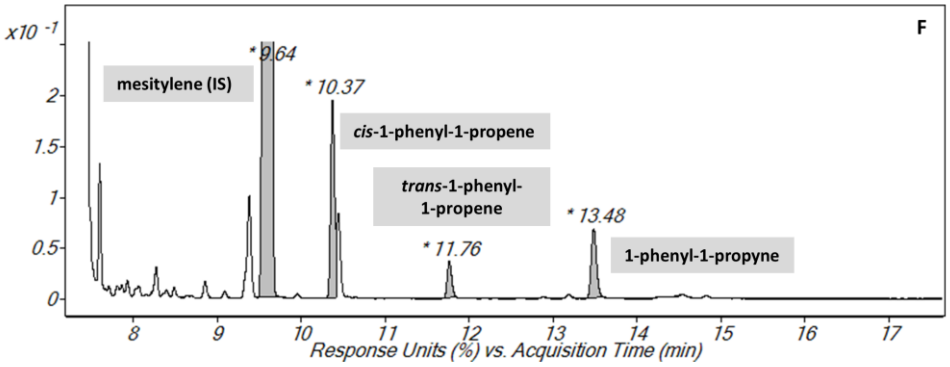
F
x10 -1
mesitylene (IS)
* 9.64
* 10.37
cis-1-phenyl-1-propene
trans-1-phenyl-1-propene
* 13.48
* 11.76
1-phenyl-1-propyne
Response Units (%) vs. Acquisition Time (min)

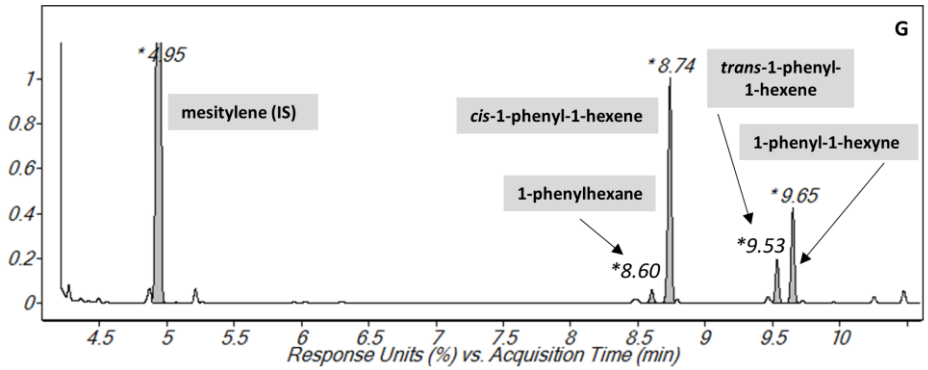
G
* 4.95
mesitylene (IS)
* 8.74
trans-1-phenyl-1-hexene
cis-1-phenyl-1-hexene
1-phenyl-1-hexyne
1-phenylhexane
* 9.65
*9.53
*8.60
Response Units (%) vs. Acquisition Time (min)

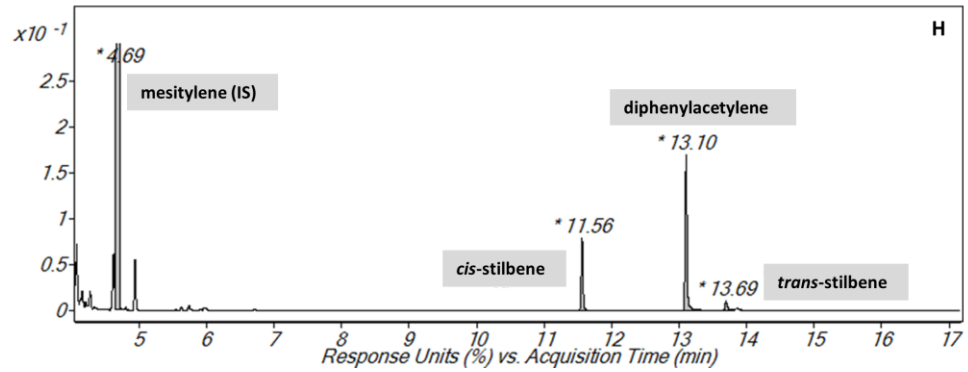
H
x10 -1
* 4.69
mesitylene (IS)
diphenylacetylene
* 13.10
* 11.56
cis-stilbene
* 13.69
trans-stilbene
Response Units (%) vs. Acquisition Time (min)

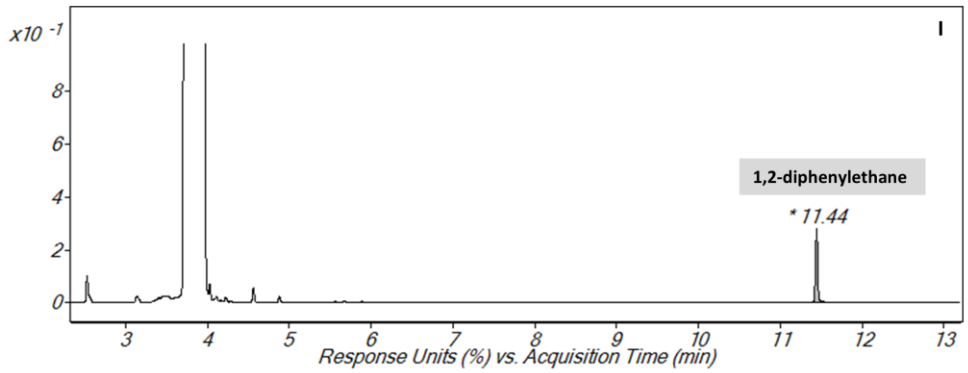
I
x10 -1
1,2-diphenylethane
* 11.44
Response Units (%) vs. Acquisition Time (min)

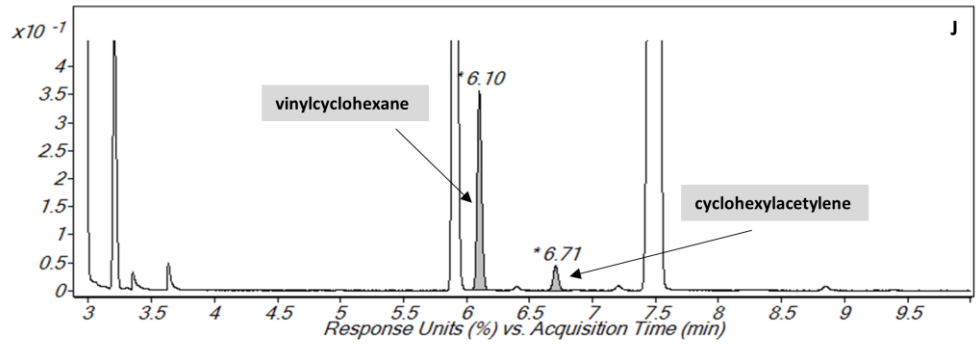
J
x10 -1
* 6.10
vinylcyclohexane
cyclohexylacetylene
* 6.71
Response Units (%) vs. Acquisition Time (min)

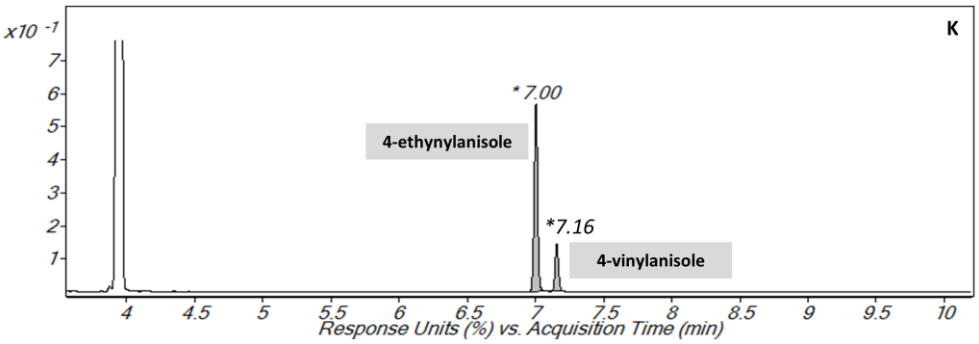
K
x10 -1
* 7.00
4-ethynylanisole
*7.16
4-vinylanisole
Response Units (%) vs. Acquisition Time (min)

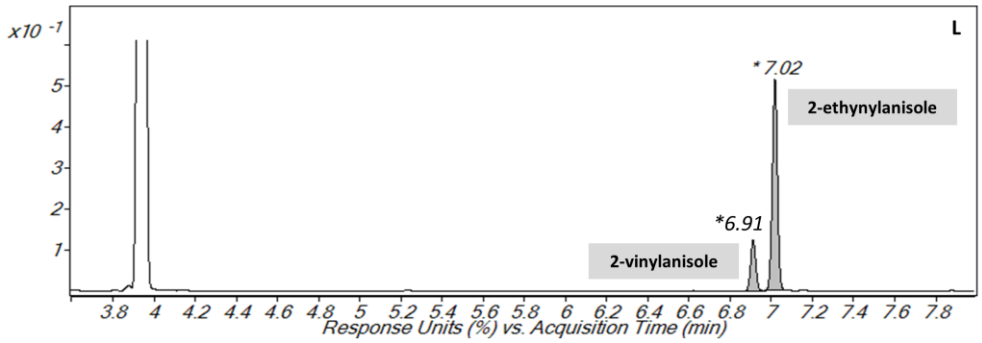

Figure S2. Representative GC spectra of substrates **1-7** and their corresponding alkene and alkane derivatives: 5-decyne (**1**) (**A-E**); 1-phenyl-1-propyne (**2**) (**F**); 1-phenyl-1-hexyne (**3**) (**G**); diphenylacetylene (**4**) (**H-I**); cyclohexylacetylene (**5**) (**J**); 4-ethynylanisole (**6**) (**K**); 2-ethynylanisole (**L**) (**7**).

Kinetic measurements, determination of activation parameters

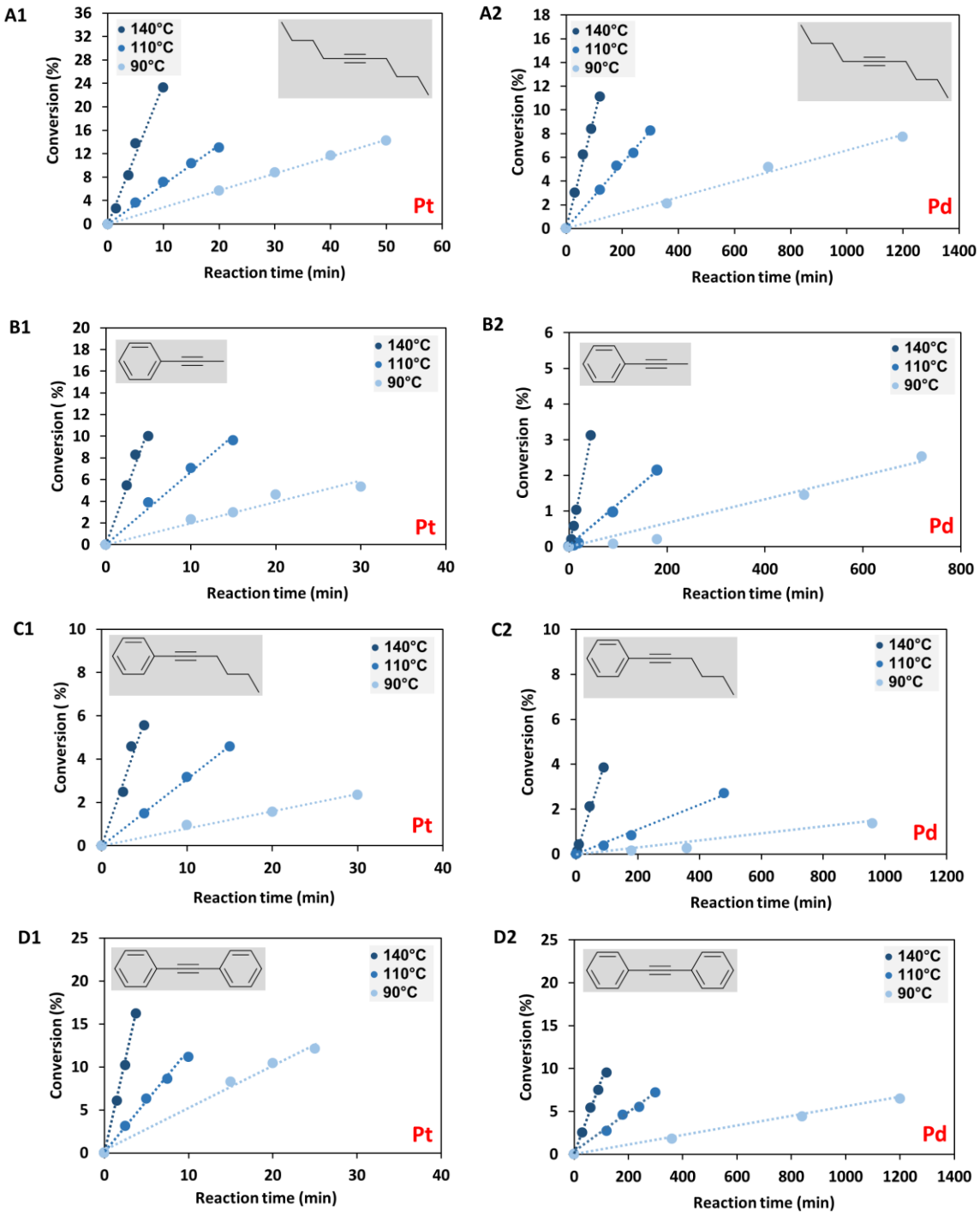

Figure S3. Hydrogen transfer of substrate **1-4** over Pt/C (**A1-D1**) and Pd/C (**A2-D2**). Reaction conditions: substrate (1.0 mmol), *p*-xylene (1.5 mL), $(^{i}Pr)_2NEt$ (4.4 mmol) over Pt/C (10 wt%, 0.1 mmol Pt) or Pd/C (10 wt%, 0.1 mmol Pd), under Ar at a given reaction temperature and reaction time. All data points of kinetic experiments were taken from separate measurements, no *in situ* sampling was applied.

Table S1. Initial rates at different reaction temperatures for substrate **1** on Pt/C ($^{i}Pr)_2NEt$).

T (°C)	T (K)	1/T (K^{-1})	r (mol $g_{(cat)}^{-1}$ s^{-1})	ln(r)	TOF (mol $mol_{(surf.\ metal)}^{-1}$ s^{-1})	ln(TOF)	ln(A)
140	413	0.00242	2.03×10^{-6}	-13.10	1.81×10^{-2}	-4.01	11.34
110	383	0.00260	5.76×10^{-7}	-14.36	5.11×10^{-3}	-5.28	
90	363	0.00275	2.46×10^{-7}	-15.21	2.19×10^{-3}	-6.13	

Table S2. Initial rates at different reaction temperatures for substrate **1** on Pd/C ($^{i}Pr)_2NEt$).

T (°C)	T (K)	1/T (K^{-1})	r (mol $g_{(cat)}^{-1}$ s^{-1})	ln(r)	TOF (mol $mol_{(surf.\ metal)}^{-1}$ s^{-1})	ln(TOF)	ln(A)
140	413	0.00242	1.48×10^{-7}	-15.72	7.44×10^{-4}	-7.20	12.35
110	383	0.00260	4.31×10^{-8}	-16.96	2.16×10^{-4}	-8.44	
90	363	0.00275	9.86×10^{-9}	-18.43	4.96×10^{-5}	-9.91	

Table S3. Initial rates at different reaction temperatures for substrate **2** on Pt/C ($^{i}Pr)_2NEt$).

T (°C)	T (K)	1/T (K^{-1})	r (mol $g_{(cat)}^{-1}$ s^{-1})	ln(r)	TOF (mol $mol_{(surf.\ metal)}^{-1}$ s^{-1})	ln(TOF)	ln(A)
140	413	0.00242	1.81×10^{-6}	-13.22	1.21×10^{-2}	-4.41	12.79
110	383	0.00260	5.71×10^{-7}	-14.37	3.80×10^{-3}	-5.57	
90	363	0.00275	1.68×10^{-7}	-15.59	1.12×10^{-3}	-6.79	

Table S4. Initial rates at different reaction temperatures for substrate **2** on Pd/C ($^{i}Pr)_2NEt$).

T (°C)	T (K)	1/T (K^{-1})	r (mol $g_{(cat)}^{-1}$ s^{-1})	ln(r)	TOF (mol $mol_{(surf.\ metal)}^{-1}$ s^{-1})	ln(TOF)	ln(A)
140	413	0.00242	1.07×10^{-7}	-16.05	7.00×10^{-4}	-7.26	14.57
110	383	0.00260	1.81×10^{-8}	-17.82	1.81×10^{-4}	-9.04	
90	363	0.00275	5.32×10^{-9}	-19.05	3.48×10^{-5}	-10.27	

Table S5. Initial rates at different reaction temperatures for substrate **3** on Pt/C ($^{i}Pr)_2NEt$).

T (°C)	T (K)	1/T (K^{-1})	r (mol $g_{(cat)}^{-1}$ s^{-1})	ln(r)	TOF (mol $mol_{(surf.\ metal)}^{-1}$ s^{-1})	ln(TOF)	ln(A)
140	413	0.00242	9.81×10^{-7}	-13.83	6.54×10^{-3}	-5.03	14.30
110	383	0.00260	2.63×10^{-7}	-15.14	1.76×10^{-3}	-6.34	
90	363	0.00275	6.78×10^{-8}	-16.50	4.52×10^{-4}	-7.70	

Table S6. Initial rates at different reaction temperatures for substrate **3** on Pd/C ($^{i}Pr)_2NEt$).

T (°C)	T (K)	1/T (K^{-1})	r (mol $g_{(cat)}^{-1}$ s^{-1})	ln(r)	TOF (mol $mol_{(surf.\ metal)}^{-1}$ s^{-1})	ln(TOF)	ln(A)
140	413	0.00242	6.83×10^{-8}	-16.49	4.45×10^{-4}	-7.71	17.30
110	383	0.00260	8.61×10^{-9}	-18.57	5.62×10^{-5}	-9.78	
90	363	0.00275	2.19×10^{-9}	-19.93	1.43×10^{-5}	-11.15	

Table S7. Initial rates at different reaction temperatures for substrate **4** on Pt/C ($^{i}Pr)_2$NEt).

T (°C)	T (K)	1/T (K^{-1})	r ($mol\ g_{(cat)}^{-1}\ s^{-1}$)	ln(r)	TOF ($mol\ mol_{(surf.\ metal)}^{-1}\ s^{-1}$)	ln(TOF)	ln(A)
140	413	0.00242	3.61×10^{-6}	-12.53	3.20×10^{-2}	-3.44	11.38
110	383	0.00260	9.83×10^{-7}	-13.83	8.72×10^{-3}	-4.74	
90	363	0.00275	4.72×10^{-7}	-14.56	4.19×10^{-3}	-5.47	

Table S8. Initial rates at different reaction temperatures for substrate **4** on Pd/C ($^{i}Pr)_2$NEt).

T (°C)	T (K)	1/T (K^{-1})	r ($mol\ g_{(cat)}^{-1}\ s^{-1}$)	ln(r)	TOF ($mol\ mol_{(surf.\ metal)}^{-1}\ s^{-1}$)	ln(TOF)	ln(A)
140	413	0.00242	1.28×10^{-7}	-15.86	7.19×10^{-4}	-7.24	12.53
110	383	0.00260	3.72×10^{-8}	-17.10	2.09×10^{-4}	-8.47	
90	363	0.00275	8.30×10^{-9}	-18.60	4.60×10^{-5}	-9.97	

Determination of activation enthalpy ($\Delta H^{\circ\ddagger}$) and activation entropy ($\Delta S^{\circ\ddagger}$)

The Eyring equation[3] with the corresponding measured TOF values were used to calculate the activation entropy and enthalpy values (k_B = Boltzmann constant (1.38×10^{-23} J K^{-1}), T = temperature (K), h = Planck constant (6.63×10^{-34} J s), R = universal gas constant (8.314 J mol^{-1} K^{-1})).

Table S9. Calculation of [ln (TOF h k_B^{-1} T^{-1}) R] values on Pt/C and Pd/C for the determination of activation entropy and enthalpy (with $^{i}Pr)_2$NEt as H-donor in *p*-xylene as solvent).

Substrate			Catalyst	
			Pt/C	Pd/C
	T (K)	$1000 \times 1/T\ (K^{-1})$	ln (TOF h k_B^{-1} T^{-1}) R	
5-decyne (1)	413	2.42	-281.00	-307.51
	383	2.61	-290.87	-317.15
	363	2.75	-297.48	-328.95
1-phenyl-1-propyne (2)	413	2.42	-284.31	-308.02
	383	2.61	-293.32	-322.15
	363	2.75	-303.02	-331.91
1-phenyl-1-hexyne (3)	413	2.42	-289.44	-311.77
	383	2.61	-299.75	-328.36
	363	2.75	-310.58	-339.29
diphenylacetylene (4)	413	2.42	-276.23	-307.79
	383	2.61	-286.42	-317.45
	363	2.75	-292.07	-329.49

Reaction order determination of substrate 1-4

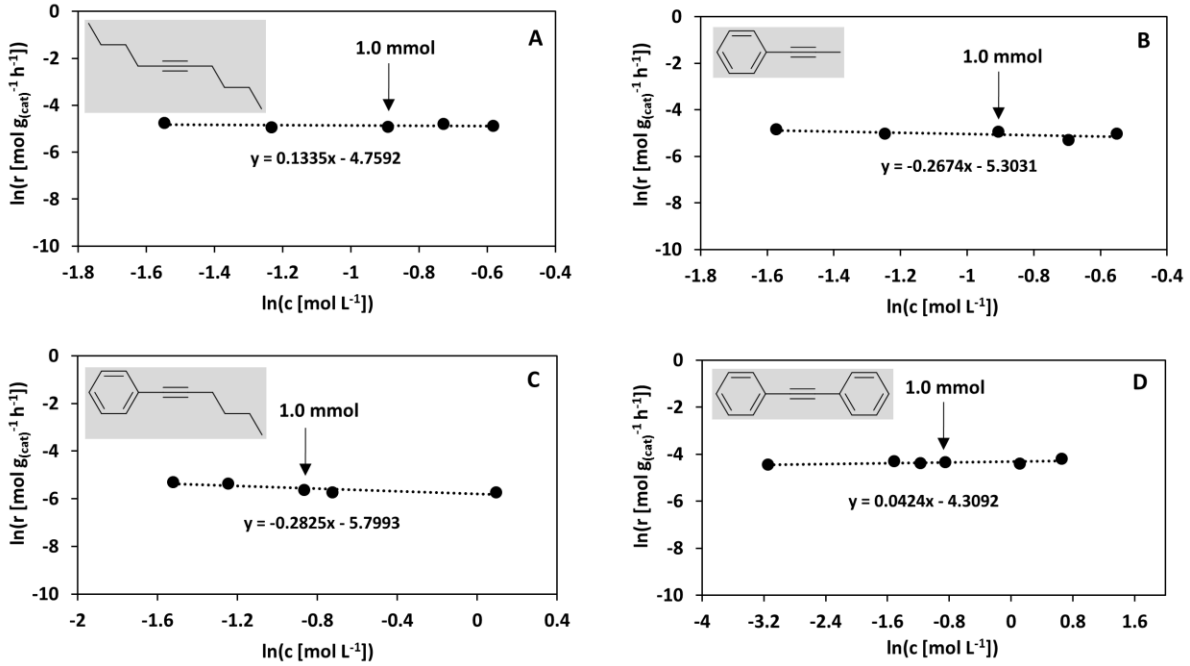

Figure S4. Reaction order determination of substrate **1** (**A**), **2** (**B**), **3** (**C**) and **4** (**D**) on Pt/C, in the presence of $(^{i}Pr)_2NEt$ at 140°C under inert conditions. All data points of experiments were taken from separate measurements, no *in situ* sampling was applied.

Table S10. Reaction order of 5-decyne (**1**) (substrate **1** (0.5–1.4 mmol), Pt/C (10 wt%, 0.1 mmol Pt), $(^{i}Pr)_2NEt$ (4.4 mmol), *p*-xylene (1.5 mL), 140 °C, under Ar and atmospheric pressure).

Substrate 1 (mmol)	c (mol L^{-1})	ln(c)	r (mol $g_{(cat)}^{-1}$ h^{-1})	ln(r)
0.5	0.213	-1.545	8.56×10^{-3}	-4.76
0.7	0.291	-1.232	7.08×10^{-3}	-4.95
1.0	0.410	-0.890	7.31×10^{-3}	-4.92
1.2	0.483	-0.727	8.29×10^{-3}	-4.79
1.4	0.559	-0.581	7.55×10^{-3}	-4.88

Table S11. Reaction order of 1-phenyl-1-propyne (**2**) (substrate **2** (0.5–1.4 mmol), Pt/C (10 wt%, 0.1 mmol Pt), $(^{i}Pr)_2NEt$ (4.4 mmol), *p*-xylene (1.5 mL), 140 °C, under Ar and atmospheric pressure).

Substrate 2 (mmol)	c (mol L^{-1})	ln(c)	r (mol $g_{(cat)}^{-1}$ h^{-1})	ln(r)
0.5	0.207	-1.572	7.84×10^{-3}	-4.85
0.7	0.287	-1.246	6.49×10^{-3}	-5.04
1.0	0.404	-0.905	6.54×10^{-3}	-5.03
1.2	0.499	-0.694	4.94×10^{-3}	-5.31
1.4	0.576	-0.550	6.45×10^{-3}	-5.04

Table S12. Reaction order of 1-phenyl-1-hexyne (**3**) (substrate **3** (0.5–3.0 mmol), Pt/C (10 wt%, 0.1 mmol Pt), (^{i}Pr)$_2$NEt (4.4 mmol), *p*-xylene (1.5 mL), 140 °C, under Ar and atmospheric pressure).

Substrate 3 (mmol)	c (mol L^{-1})	ln(c)	r (mol $g_{(cat)}^{-1}$ h^{-1})	ln(r)
0.5	0.218	-1.519	4.92×10^{-3}	-5.31
0.7	0.287	-1.244	4.67×10^{-3}	-5.36
1.0	0.421	-0.864	3.53×10^{-3}	-5.64
1.2	0.485	-0.722	3.23×10^{-3}	-5.73
3.0	1.100	-0.096	3.22×10^{-3}	-5.73

Table S13. Reaction order of diphenylacetylene (**4**) (substrate **4** (0.1–6.0 mmol), Pt/C (10 wt%, 0.1 mmol Pt), (^{i}Pr)$_2$NEt (4.4 mmol), *p*-xylene (1.5 mL), 140 °C, under Ar and atmospheric pressure).

Substrate 4 (mmol)	c (mol L^{-1})	ln(c)	r (mol $g_{(cat)}^{-1}$ h^{-1})	ln(r)
0.1	0.043	-3.146	11.68×10^{-3}	-4.45
0.5	0.221	-1.508	13.42×10^{-3}	-4.31
0.7	0.309	-1.173	12.41×10^{-3}	-4.39
1.0	0.426	-0.851	12.99×10^{-3}	-4.34
3.0	1.118	-0.112	12.12×10^{-3}	-4.41
6.0	1.925	-0.655	14.97×10^{-3}	-4.20

Reaction order determination of (^{i}Pr)$_2$NEt and 1-EPyr in the presence of substrate 4

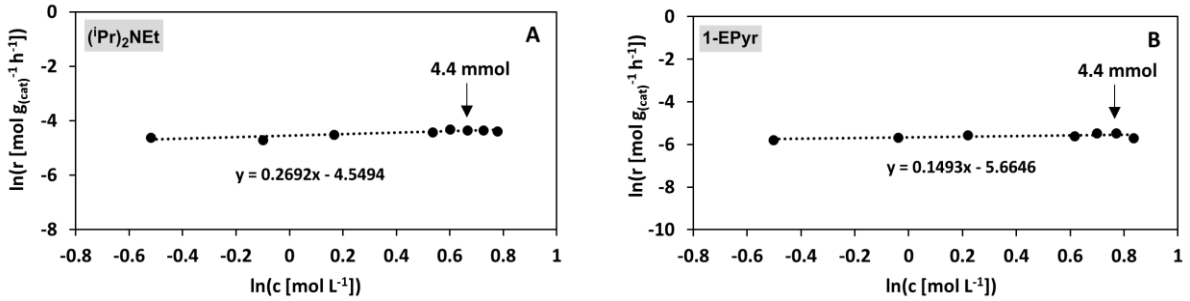

Figure S5. Reaction order determination of (^{i}Pr)$_2$NEt (**A**) and 1-EPyr (**B**) at 140°C on Pt/C, in *p*-xylene as solvent under inert conditions in the presence of substrate **4**. All data points of experiments were taken from separate measurements, no *in situ* sampling was applied.

Table S14. Reaction order of (^{i}Pr)$_2$NEt (substrate **4** (1.0 mmol), Pt/C (10 wt%, 0.1 mmol Pt), (^{i}Pr)$_2$NEt (1.0–5.2 mmol), *p*-xylene (1.5 mL), 140 °C, under Ar and atmospheric pressure).

Amine ((^{i}Pr)$_2$NEt) (mmol)	c (mol L^{-1})	ln(c)	r (mol $g_{(cat)}^{-1}$ h^{-1})	ln(r)
1.0	0.594	-0.519	9.96×10^{-3}	-4.61
1.6	0.905	-0.099	9.01×10^{-3}	-4.71
2.2	1.180	0.166	11.07×10^{-3}	-4.50
3.6	1.708	0.535	11.91×10^{-3}	-4.43
4.0	1.822	0.600	13.37×10^{-3}	-4.31
4.4	1.947	0.666	12.99×10^{-3}	-4.34
4.8	2.064	0.725	13.02×10^{-3}	-4.34
5.2	2.175	0.777	12.54×10^{-3}	-4.38

Table S15. Reaction order of 1-EPyr (substrate **4** (1.0 mmol), Pt/C (10 wt%, 0.1 mmol Pt), 1-EPyr (1.0–4.8 mmol), *p*-xylene (1.5 mL), 140 °C, under Ar and atmospheric pressure).

Amine (1-EPyr) (mmol)	c (mol L^{-1})	ln(c)	r (mol $g_{(cat)}^{-1}$ h^{-1})	ln(r)
1.0	0.605	-0.502	3.09×10^{-3}	-5.78
1.6	0.960	-0.039	3.43×10^{-3}	-5.67
2.2	1.245	0.219	3.85×10^{-3}	-5.56
3.6	1.852	0.616	3.63×10^{-3}	-5.62
4.0	2.011	0.698	4.18×10^{-3}	-5.48
4.4	2.162	0.771	4.19×10^{-3}	-5.47
4.8	2.305	0.835	3.38×10^{-3}	-5.69

Computational details

General calculation details All DFT calculations were performed using periodic boundary conditions in the *Vienna Ab Initio Simulation Program* (VASP) version 5.4.[4] The Perdew-Berke-Ernzerhof (PBE) exchange-correlation functional[5] was used with the projector-augmented wave (PAW) method[6] to describe electron-ion interactions. Dispersion corrections were added using Grimme's DFT-D3 method with Becke-Johnson damping.[7] An energy cutoff of 500 eV was used for the plane wave basis set in all calculations. First-order Methfessel-Paxton smearing[8] (σ = 0.2 eV) was used to describe the partial occupancies. Convergence criteria of 10^{-6} eV was used for the total energy, while the break condition for the optimization was set at 10^{-5} eV. For all slab calculations, the projection operators were evaluated in real space.

Slab models The catalytic surface was modeled using the (111) facet of Pt and Pd. First, bulk optimizations were performed to optimize the lattice vectors at the chosen level of theory. A gamma-centered k-point grid of 12×12x12 resulted in convergence of the lattice vectors to 0.001 Å (Pt: 3.926 Å; Pt 3.887 Å). These lattice vectors were used to generate four-layer slabs of the fcc metals with a (111) surface facet. In all calculations with these surfaces, the top two layers were allowed to relax while the bottom two (and the lattice vectors) were kept frozen to maintain the bulk structure. A vacuum spacer of 20 Å was used to prevent interactions with the underside of the surface. A gamma-centered k-point grid of 3×3x1 was used for all surface calculations.

Binding energy calculations Binding energies were computed using the expression (**Eq S1**)

$$E_{bind} = E_{surface+molecule} - (E_{surface} + E_{molecule}) \qquad \textbf{(Eq S1)}$$

where $E_{surface}$ is the electronic energy of the metal slab, $E_{molecule}$ is the electronic energy of the isolated adsorbate molecule, and $E_{surface+molecule}$ is the electronic energy of the adsorbate bound on the surface. To obtain the energies of the isolated adsorbates, molecules were optimized at the center of a 20×20x20 $Å^3$ periodic box with a k-point grid consisting of only the gamma point.

Models of surface coverage For calculations of the transfer hydrogenation of **2** by 1-EPyr on Pt, we used surfaces of two different sizes to model higher effective surface coverage. A periodic cell of size 4×4 was used to model higher amine surface coverage, while a 4×5 model was used for the lower coverage situation (**Figure S9**). The validity of using different cell sizes to model the coverage was confirmed by checking that the *cis-trans* isomerization energy was converged to 0.1 eV when compared to a larger 8×8 supercell with four alkyne and amine molecules. Calculations at even higher coverage (3×4 cell) were also performed and showed a nearly equivalent energy difference between the two (*cis*/*trans*-) metal hydride-alkylamine yne/ene isomers (yne/ene refers to the semi saturation state of the alkyne) to that in the 4×4 case; however, these results were excluded from consideration because the alkene does not form at such high coverages (phenyl group cannot lie on surface).

Structural and electronic effects of 1-EPyr on the *cis-trans* selectivity of substrate 2 (1-phenyl-1-propyne) hydrogenation The presence of 1-EPyr on the surface has two major effects on the metal hydride-alkylamine yne/ene intermediates: (1) structural distortions due to steric interactions between the alkyne and amine and (2) an electronic effect that may stabilize either the *cis* or *trans* isomer. We broke this structural effect into two

components $E_{struct,alkyne}$ corresponding to the energetic effect of distortions on the alkyne, and $E_{struct,other}$ corresponding to the effect of structural distortions on the energetics of the rest of the system (i.e. amine and surface). Both of these effects were computed by removing components from the optimized structures of the combined system. To calculate $E_{struct,alkyne}$ 1-EPyr was removed from the optimized structure. Then, the geometry of the alkyne was frozen while the rest of the system was allowed to relax, isolating only those structural distortions to the alkyne caused by the amine. The energy difference between the structure with the constrained alkyne geometry and a fully optimized structure in the absence of amine is reported as $E_{struct,alkyne}$ (**Table S16**). To determine the effect of structural distortion on the rest of the system, a single point calculation was performed on the optimized structure for the combined system with the alkyne removed. The difference between these single point energies and that of an optimized metal hydride-alkylamine structure (without alkyne) gave $E_{struct,other}$ (**Table S16**). Combining these two effects gave $E_{struct,total}$ the total effect of structural distortions on the energetics.

To isolate the electronic effect of the 1-EPyr on the *cis-trans* selectivity, we used the following expression (**Eq S2**):

$$\Delta E_{cis\text{-}trans,amine} = \Delta E_{cis\text{-}trans,struct} + \Delta E_{cis\text{-}trans,elect} \qquad \textbf{(Eq S2)}$$

where $\Delta E_{cis\text{-}trans,amine}$ is the total shift in the relative energy of the *cis* and *trans* isomers due to the amine, $\Delta E_{cis\text{-}trans,struct}$ is the shift in their relative energetics from structural distortions, and $\Delta E_{cis\text{-}trans,elect}$ is the shift due to the electronic effect of the amine. The total shift in relative energetics due structural distortions is given by (**Eq S3**)

$$\Delta E_{cis\text{-}trans,struct} = E_{struct,total}[cis] - E_{struct,total}[trans] \qquad \textbf{(Eq S3)}$$

while the total effect of the amine ($\Delta E_{cis\text{-}trans,amine}$) is simply the difference between the *cis-trans* isomerization energy with the amine and that for the isolated intermediate. Values for each of these quantities are reported in **Table S17**.

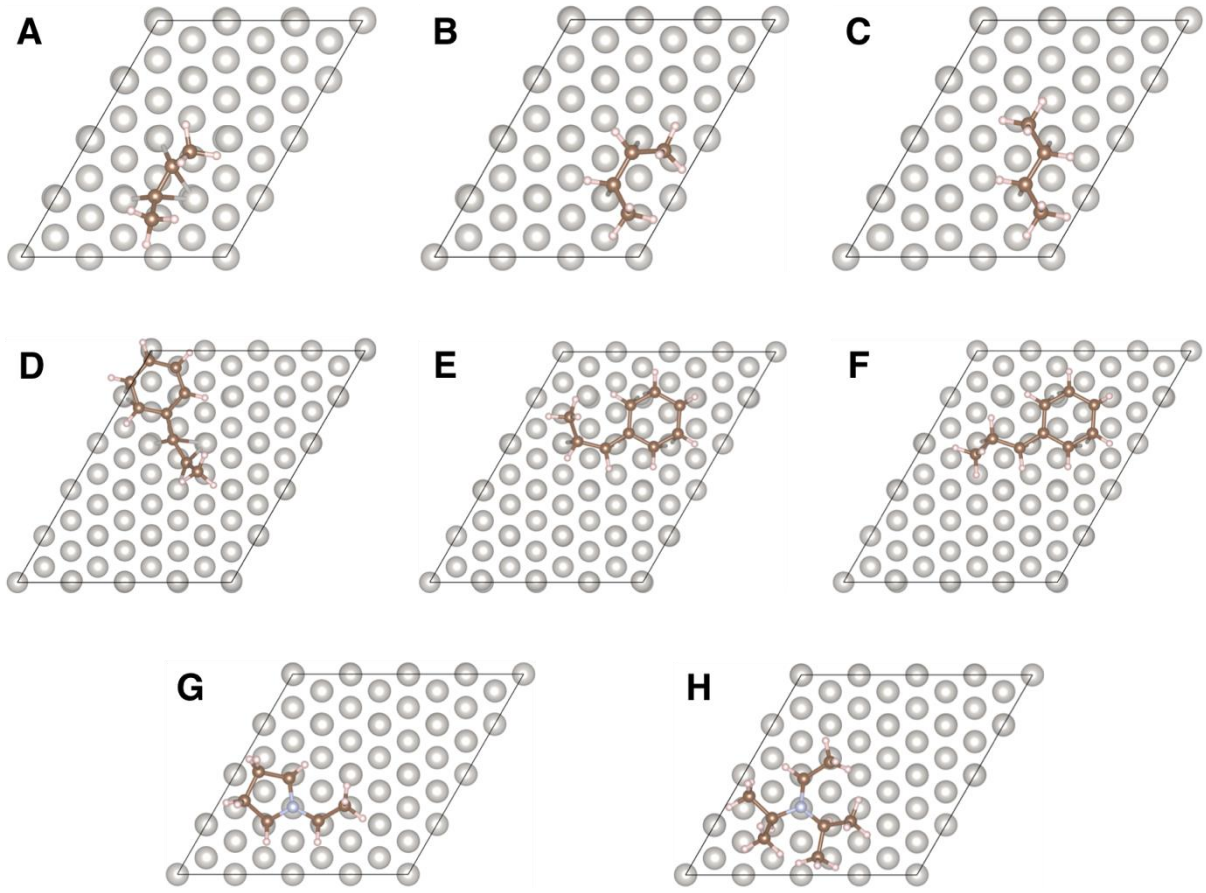

Figure S6. Minimum energy binding geometries of alkynes, alkenes and amines on Pt(111) surface. (**A**) 2-butyne; (**B**) *cis*-2-butene; (**C**) *trans*-2-butene; (**D**) 1-phenyl-1-propyne; (**E**) *cis*-1-phenyl-1-propene; (**F**) *trans*-1-phenyl-1-propene; (**G**) 1-EPyr; (**H**) $(^{i}Pr)_2NEt$.

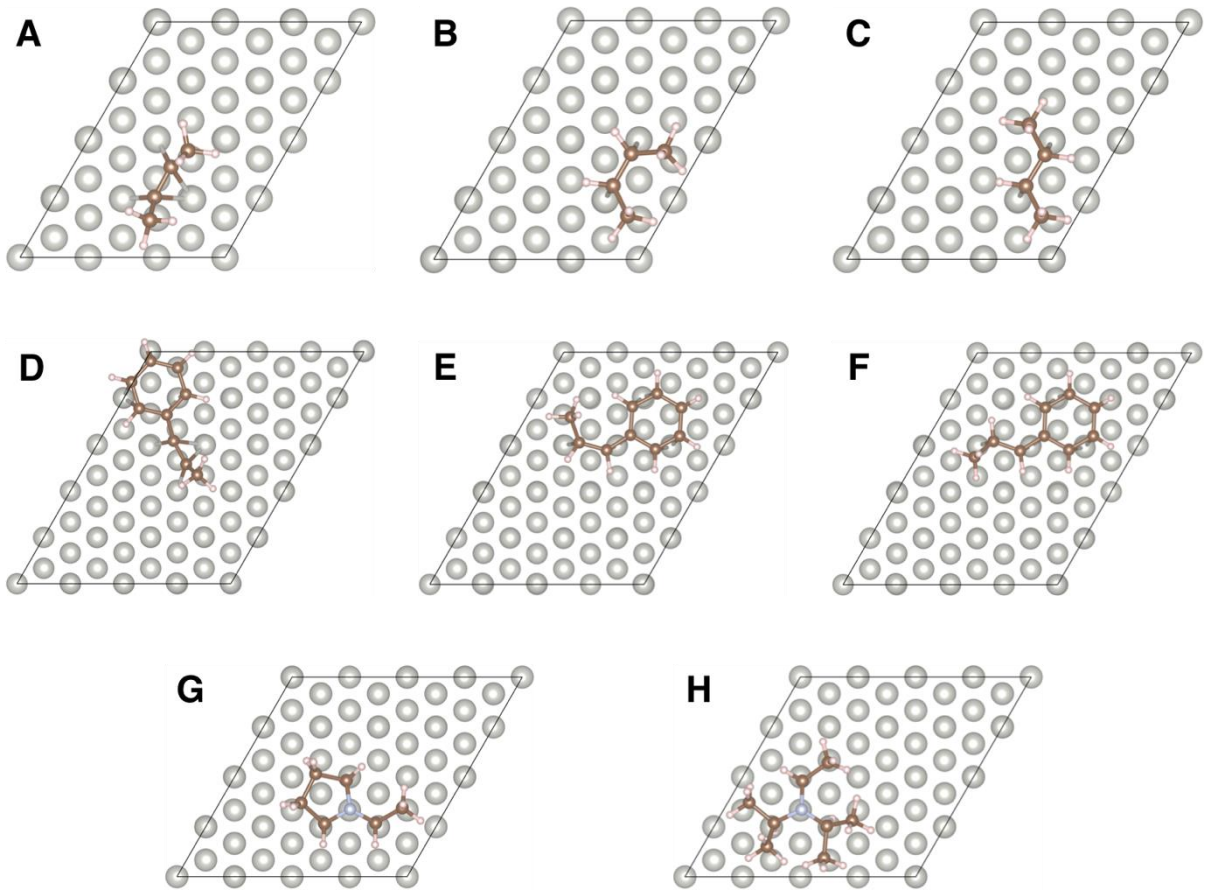

Figure S7. Minimum energy binding geometries of alkynes, alkenes and amines on Pd(111) surface. (**A**) 2-butyne; (**B**) *cis*-2-butene; (**C**) *trans*-2-butene; (**D**) 1-phenyl-1-propyne; (**E**) *cis*-1-phenyl-1-propene; (**F**) *trans*-1-phenyl-1-propene; (**G**) 1-EPyr; (**H**) $(^{i}Pr)_2NEt$.

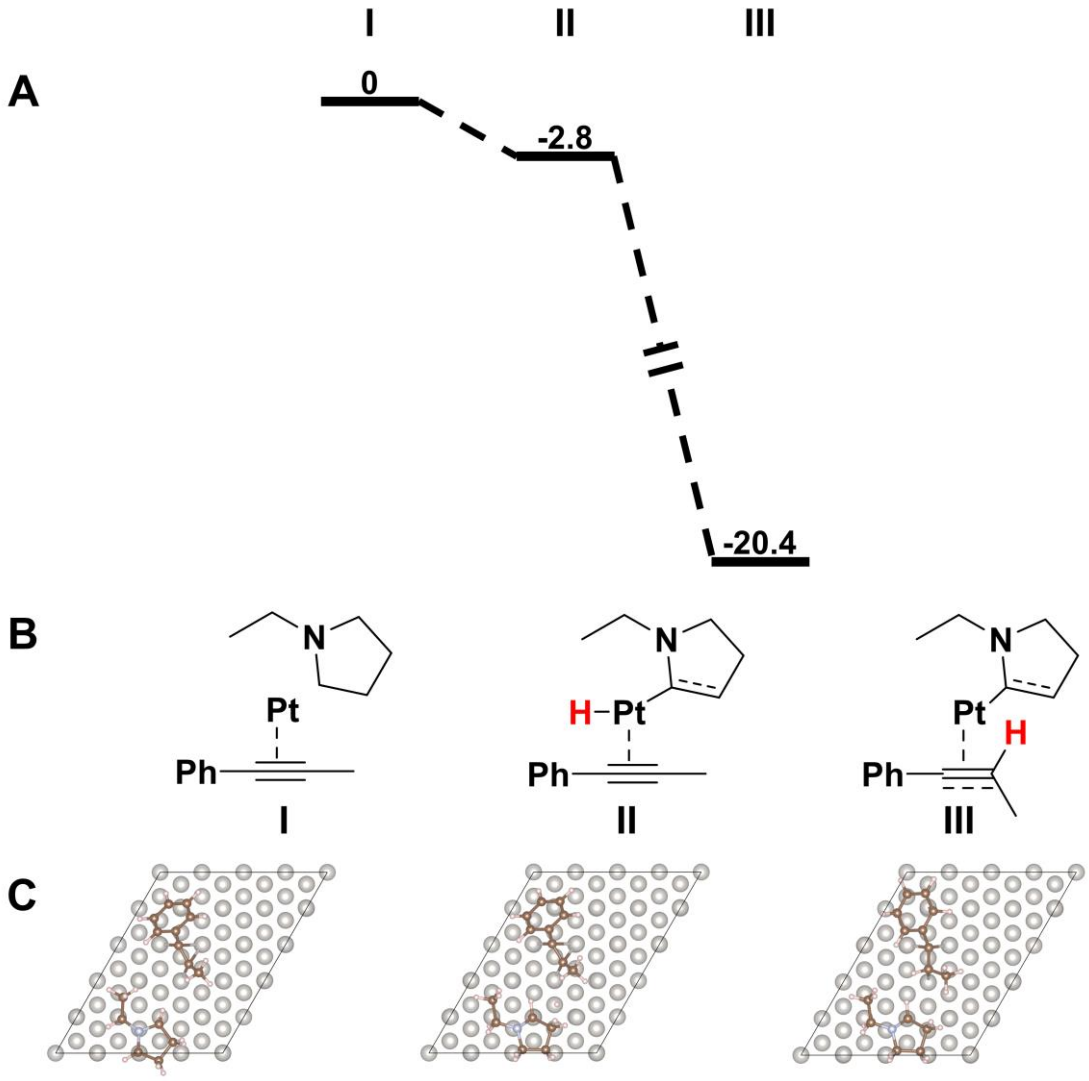

Figure S8. (**A**) Reaction energetics (in kJ mol^{-1}) for the first transfer hydrogenation step from 1-EPyr to **2** on Pt(111). This involves H transfer from 1-EPyr to Pt to form a metal hydride-alkylamine alkyne intermediate (**I→II**) followed by H transfer from Pt to **2** to form a (mono-hydrogenated) metal-alkylamine yne/ene intermediate (**II→III**). (**B**) Schematic and (**C**) minimum energy structures of the reaction intermediates.

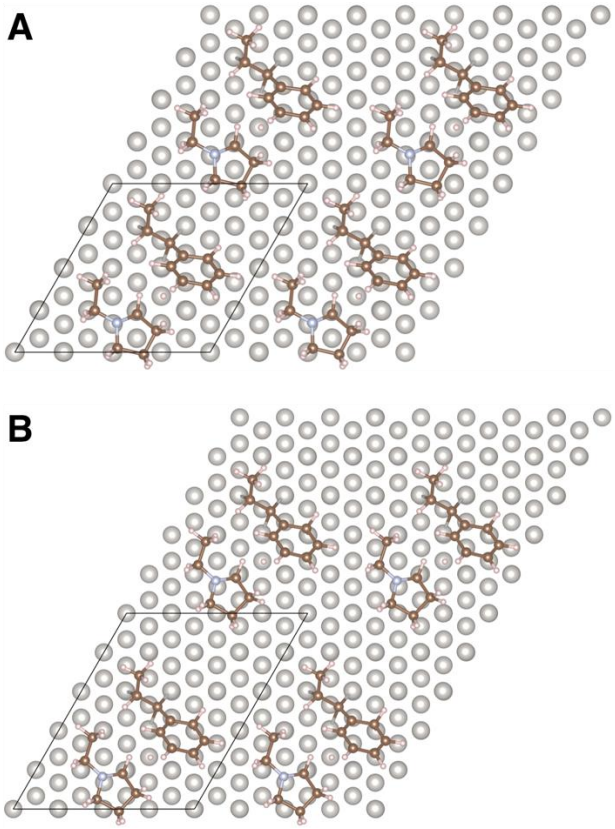

Figure S9. Minimum energy structures of the (mono-hydrogenated) *cis* yne/ene Pt hydride-alkylamine intermediate for the (**A**) high and (**B**) low coverage surface models (a×b = 4×4 and 4×5, respectively). The unit cells (black line) are repeated in the x and y direction to show the closer packing between the alkyne (**2**) and the amine (1-EPyr) in the high coverage case.

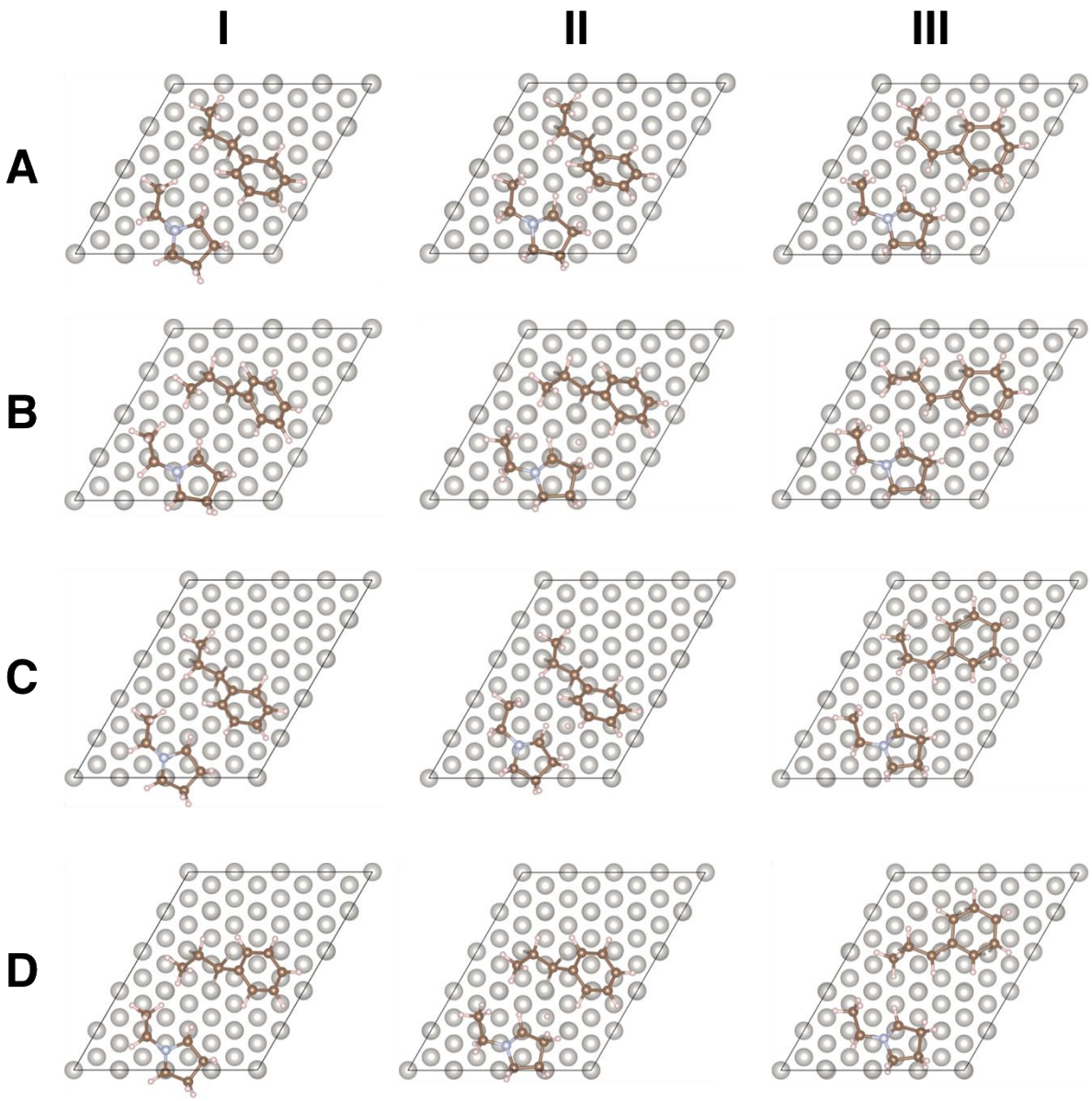

Figure S10. Minimum energy intermediates for the transfer hydrogenation of **2** by 1-EPyr on Pt. Intermediates are labeled (**I**, **II**, **III**) according to the schematic in **Figure 7C**. Each row corresponds to a different isomer and coverage level: (**A**) *cis* isomer at high coverage, (**B**) *trans* isomer at high coverage, (**C**) *cis* isomer at low coverage, (**D**) *trans* isomer at low coverage.

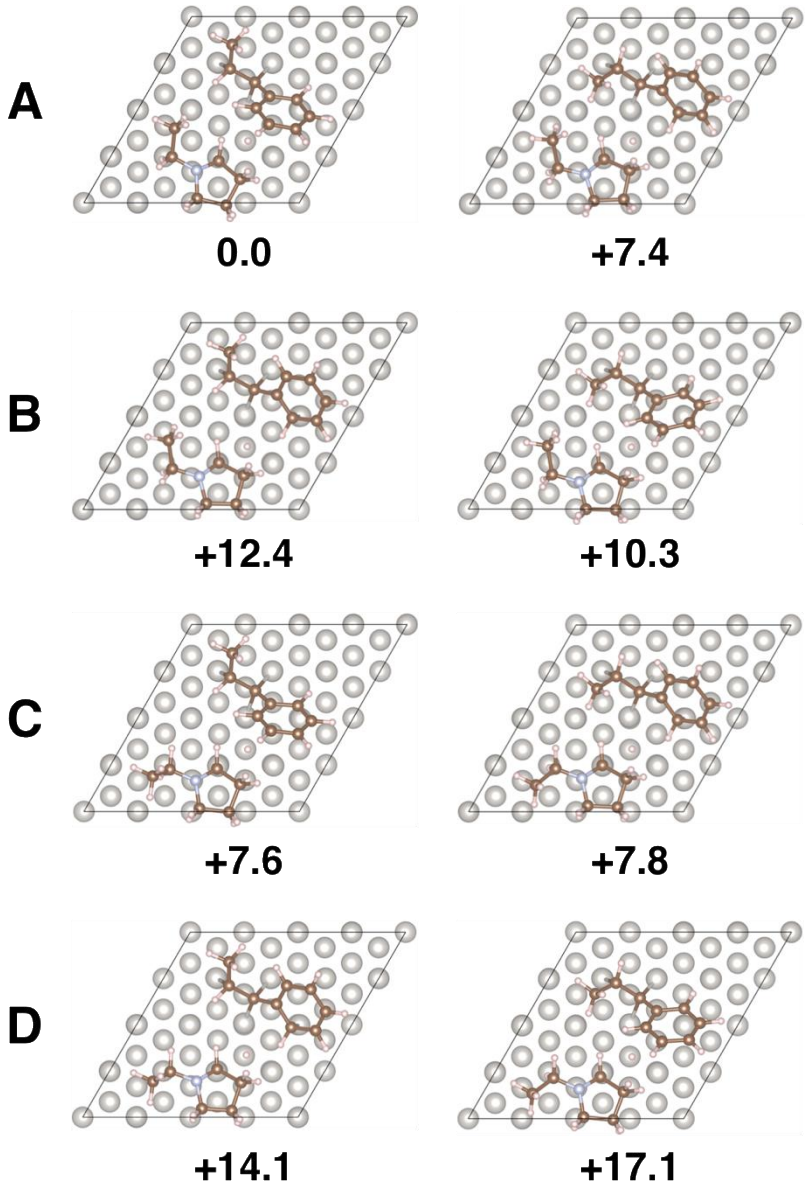

Figure S11. Representative alternative binding conformations for *cis* (left) and *trans* (right) (mono-hydrogenated) Pt hydride-alkylamine yne/ene intermediates in the transfer hydrogenation of **2** by 1-EPyr on Pt at high coverage. The relative energy of each conformation relative to the minimum energy *cis* intermediate is given under each structure (in kJ mol^{-1}). Other conformations were too unstable to warrant inclusion. These geometries correspond to (**A**) minimum energy conformers, (**B**) rotated phenyl group on **2**, (**C**) rotated ethyl group on 1-EPyr, (**D**) both rotated phenyl group on **2** and rotated ethyl group on 1-EPyr.

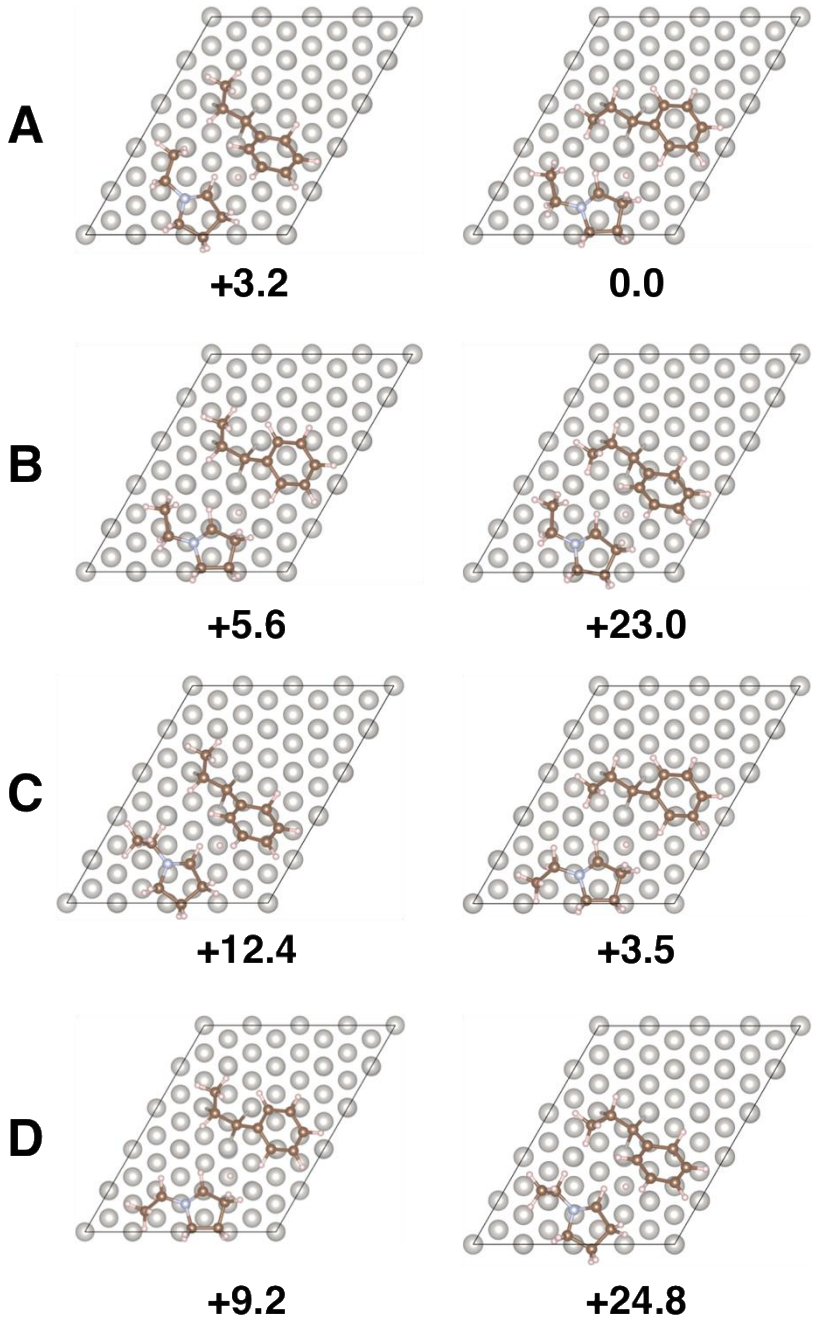

Figure S12. Alternative binding conformations for *cis* (left) and *trans* (right) (mono-hydrogenated) Pt hydride-alkylamine yne/ene intermediates in the transfer hydrogenation of **2** by 1-EPyr on Pt at low coverage. The relative energy of each conformation relative to the minimum energy *trans* intermediate is given under each structure (in kJ mol^{-1}). Other conformations were too unstable to warrant inclusion. These geometries correspond to (**A**) minimum energy conformers, (**B**) rotated phenyl group on **2**, (**C**) rotated ethyl group on 1-EPyr, (**D**) both rotated phenyl group on **2** and rotated ethyl group on 1-EPyr.

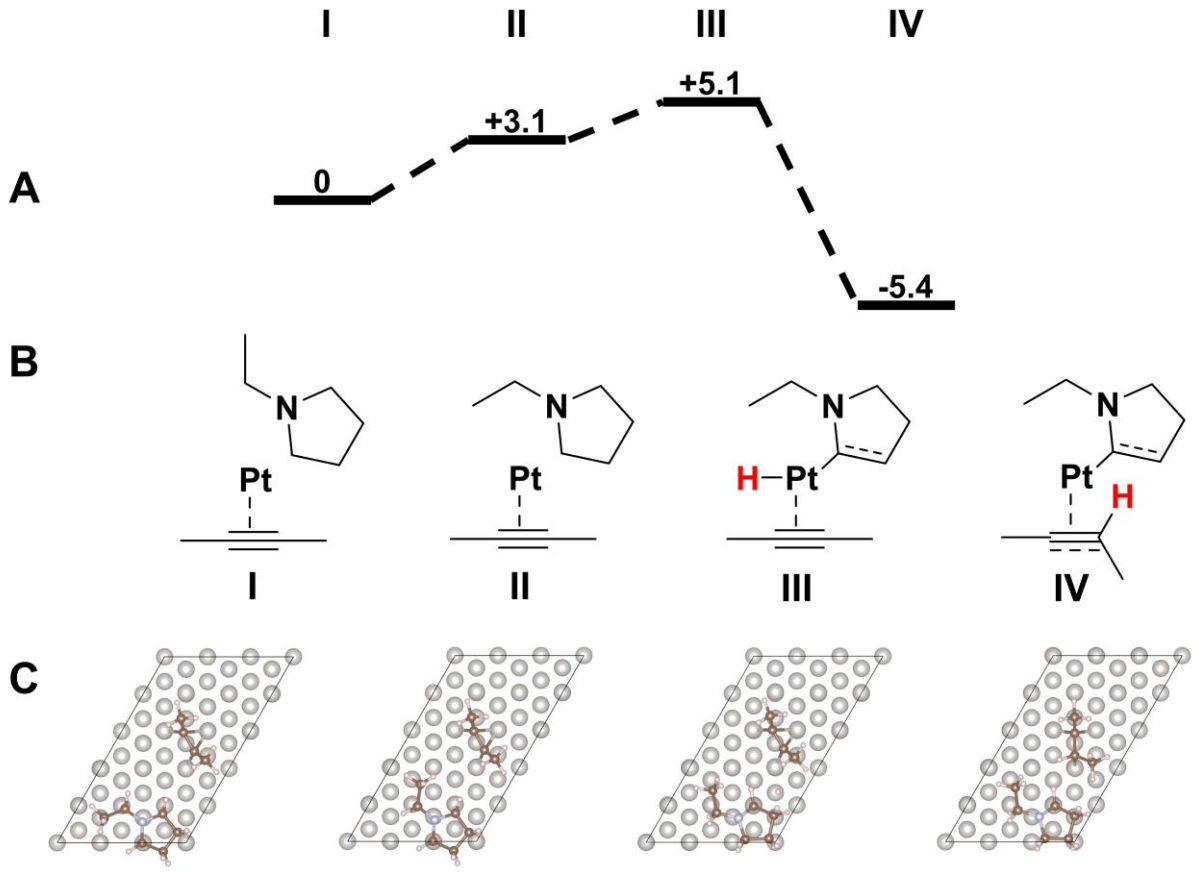

Figure S13. (**A**) Reaction energetics (in kJ mol^{-1}) for the first transfer hydrogenation step from 1-EPyr to 2-butyne on Pt(111). The reaction steps include: rotation of the ethyl group of 1-EPyr (**I→II**), H transfer from 1-EPyr to Pt to form a metal hydride-alkylamine yne/ene intermediate (**II→III**), and H transfer from Pt to 2-butyne to form a (mono-hydrogenated) Pt-alkylamine yne/ene intermediate (**III→IV**). Note that the ethyl group rotation is included because the lowest energy conformer (**I**) does not transfer H as readily as **II**. (**B**) Schematic and (**C**) minimum energy structures of the reaction intermediates.

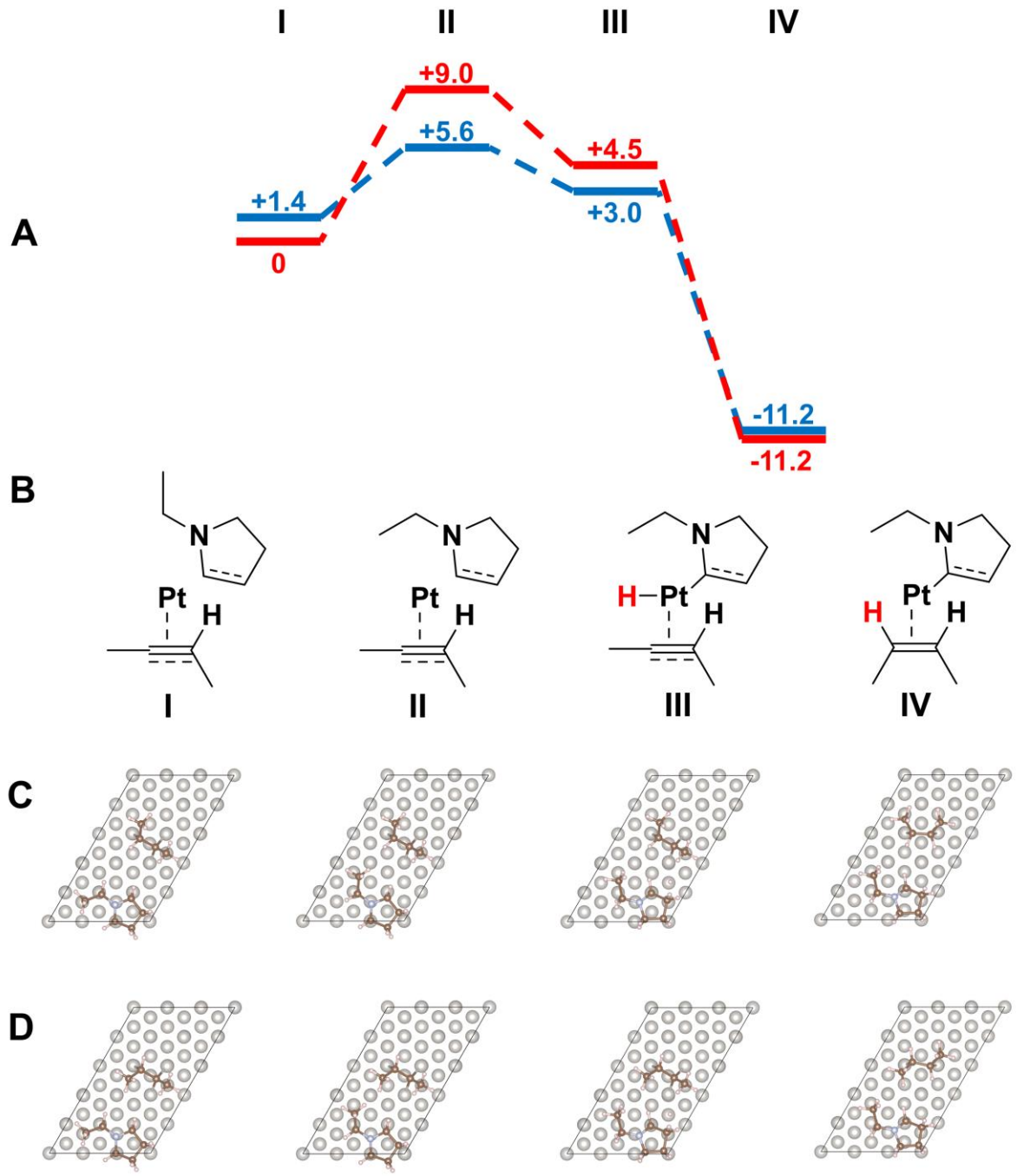

Figure S14. (**A**) Reaction energetics (in kJ mol^{-1}) for the second transfer hydrogenation step from 1-EPyr to 2-butyne on Pt(111). The pathway to form *cis* 2-butene is shown in blue, while the one producing *trans* 2-butene is shown in red. The reaction steps include: rotation of the ethyl group of 1-EPyr (**I→II**), H transfer from 1-EPyr to Pt to form a metal hydride-alkylamine yne/ene intermediate (**II→III**), and H transfer from Pt to the mono-hydrogenated alkyne intermediate to form 2-butene (**III→IV**). Note that the ethyl group rotation is included because the lowest energy conformer (**I**) does not transfer H as readily as **II**. (**B**) Schematic of reaction intermediates. (**C**) Minimum energy structures of intermediates **I** through **IV** for the *cis* pathway. (**D**) Minimum energy structures of intermediates **I** through **IV** for the *trans* pathway.

Table S16. Effects of structural distortions on the energetics of the corresponding (mono-hydrogenated) Pt hydride-alkylamine yne/ene intermediates in the transfer hydrogenation of **2** by 1-EPyr. (Each energy term is defined in the *Computational Details* section.)

Isomer	Coverage	$E_{struct,alkyne}$ (kJ mol^{-1})	$E_{struct,other}$ (kJ mol^{-1})	$E_{struct,total}$ (kJ mol^{-1})
Cis	High	+11.2	+18.7	+29.9
Trans	High	+7.6	+19.4	+27.0
Cis	Low	+14.1	+16.4	+30.6
Trans	Low	+2.1	+19.3	+21.3

Table S17. Effects of the amine on the *cis-trans* energy difference of the (mono-hydrogenated) Pt hydride-alkylamine yne/ene intermediates in the transfer hydrogenation of **2** by 1-EPyr. (Each energy term is defined in the *Computational Details* section.)

Coverage	$\Delta E_{cis\text{-}trans,amine}$ (kJ mol^{-1})	$\Delta E_{cis\text{-}trans,struct}$ (kJ mol^{-1})	$\Delta E_{cis\text{-}trans,elect}$ (kJ mol^{-1})
High	-8.2	+2.9	-11.1
Low	+0.9	+9.2	-8.3

References

1 Yang, G.; Bauer, T. J.; Haller, G. L.; Baráth, E. H-Transfer reactions of internal alkenes with tertiary amines as H-donors on carbon supported noble metals. *Org. Biomol. Chem.* **2018**, *16*, 1172–1177.

2 Perea-Buceta, J. E.; Fernández, I.; Heikkinen, S.; Axenov, K.; King, A. W. T.; Niemi, T.; Nieger, M.; Leskelä, M.; Repo, T. Diverting Hydrogenations with Wilkinson's Catalyst towards Highly Reactive Rhodium(I) Species. *Angew. Chem. Int. Ed.* **2015**, *54*, 14321–14325.

3 Hintermeier, P. H.; Eckstein, S.; Mei, D.; Olarte, M. V.; Camaioni, D. M.; Baráth, E.; Lercher, J. A. Hydronium-ion-catalyzed elimination pathways of substituted cyclohexanols in zeolite H-ZSM5. *ACS Catal.* **2017**, *7*, 7822–7829.

4 (a) Kresse, G.; Hafner, J. *Ab initio* molecular dynamics for liquid metals. *Phys. Rev. B* **1993**, *47*, 558–561. (b) Kresse, G.; Hafner, J. *Ab initio* molecular-dynamics simulation of the liquid-metal–amorphous-semiconductor transition in germanium. *Phys. Rev. B* **1994**, *49*, 14251–14269. (c) Kresse, G.; Furthmüller, J. Efficiency of *ab-initio* total energy calculations for metals and semiconductors using a plane-wave basis set. *Comput. Mater. Sci.* **1996**, *6*, 15–50. (d) Kresse, G.; Furthmüller, J. Efficient iterative schemes for *ab initio* total-energy calculations using a plane-wave basis set. *Phys. Rev. B* **1996**, *54*, 11169–11186.

5 Perdew, J. P.; Burke, K.; Ernzerhof, M. Generalized Gradient Approximation Made Simple. *Phys. Rev. Lett.* **1996**, *77*, 3865–3868.

6 (a) Blöchl, P. E. Projector augmented-wave method. *Phys. Rev. B* **1994**, *50*, 17953–17979. (b) Kresse, G.; Joubert, D. From ultrasoft pseudopotentials to the projector augmented-wave method. *Phys. Rev. B* **1999**, *59*, 1758–1775.

7 (a) Grimme, S.; Antony, J.; Ehrlich, S.; Krieg, H. A consistent and accurate *ab initio* parametrization of density functional dispersion correction (DFT-D) for the 94 elements H-Pu. *J. Chem. Phys.* **2010**, *132*, 154104. (b) Grimme, S.; Ehrlich, S.; Goerigk, L. Effect of the Damping Function in Dispersion Corrected Density Functional Theory. *J. Comput. Chem.* **2011**, *32*, 1456–1465.

8 Methfessel, M.; Paxton, A. T. High-Precision Sampling for Brillouin-zone integration in metals. *Phys. Rev. B* **1989**, *40*, 3616–3621.